PAPER

Graphene–bacteria composite for oxygen reduction and lithium ion batteries†

Xuewan Wang,[a] Wei Ai,[b] Nan Li,[a] Ting Yu[b] and Peng Chen*[a]

Owing to its extraordinary properties, graphene materials have changed the landscapes in many technical areas. However, their applications (*e.g.*, in energy conversion and storage) are often limited due to the lack of intrinsic electrochemical activity and restacking between graphene sheets. In this study, we demonstrate the synthesis of a heteroatom-doped graphene–bacteria composite using chemically-exfoliated graphene oxide as the precursor and *E. coli* as the reducing agent, spacer and doping source. As a proof-of-concept demonstration, we show that the carbonaceous rGO/*E. coli* composites are excellent electrode materials for the oxygen reduction reaction and lithium ion batteries.

1. Introduction

Owing to its large surface area, good conductivity and wide electrochemical potential window, graphene materials have been widely used for energy applications[1–3] such as oxygen reduction[4,5] and lithium ion batteries.[6,7] However, pristine graphene is not electrochemically active and lacks intrinsic catalytic abilities. Therefore, in energy devices, electrochemically active nanomaterials (*e.g.*, nanostructured metal oxides) are needed to be composited with graphene.[8–12] This complicates the synthesis process and those functional nanomaterials are not as chemically stable as graphene. Alternatively, heteroatom doping can endow graphene with good catalytic and electrochemical properties.[13–15] Nevertheless, it is often challenging to dope graphene, in particular, to co-dope multiple species of heteroatoms.

Graphene materials used in energy devices are usually prepared by chemical processes, involving oxidative chemical exfoliation from graphite and subsequent chemical reduction to restore damaged graphene lattices to a certain extent (thus impairing conductivity). Reduced graphene oxide (rGO) sheets obtained from these processes are still largely defective. In addition, the reduction processes typically involve and/or produce environmental hazards, *e.g.*, the commonly used reducing agent hydrazine. Furthermore, the restacking of rGO sheets is inevitable during chemical reduction. Mild, green, and restacking-free reduction methods are hence highly desired.

Herein, bacteria (*E. coli*) are used as an effective and environmentally friendly bio-agent to reduce GO sheets, and as spacers to prevent the restacking of the rGO sheets. As all the other living species on earth, bacteria are carbon-based lifeforms with abundant heteroatoms (especially, N, P, and S). Therefore, they may serve as good precursors and doping agents to produce doped carbon materials. We show that the thermal annealing of a graphene–bacteria composite self-assembled from the reduction process yields a porous carbon composite with abundant heteroatom species naturally inherited from the bacteria. We further demonstrate the use of such a novel graphene–bacteria composite as an electrode material for high performance oxygen reduction (ORR) and lithium ion battery (LIB) applications.

2. Experimental sections

2.1 Preparation of carbonaceous rGO/*E. coli* composite

GO was prepared from graphite powder using a modified Hummers' method.[16] *E. coli* bacteria were first inoculated into 20 mL fresh Luria broth (LB; 10 g L^{-1} tryptone, 5 g L^{-1} yeast extract, 10 g L^{-1} NaCl, pH 7.0) and were incubated overnight at 37 °C at a shaking rate of 200 rpm. 30 mg of GO was added to 150 mL of fresh LB followed by 10 min of ultrasonication (LB–GO). The cultured bacteria were harvested and re-suspended in LB–GO broth with a final optical density (OD_{600}) value of 0.3, followed by further incubation at 37 °C under aerobic conditions and a shaking rate of 200 rpm for 108 h. The resulting rGO–*E. coli* composite was collected, washed and lyophilized. Subsequently, the sample was annealed in a tube furnace in which the temperature gradually increased at 1 °C min^{-1} to 900 °C and then maintained at that temperature for 2 h. The resulting composite was washed overnight by 3 M HCl at 100 °C to remove the salts and impurities, and was finally lyophilized for use.

[a]School of Chemical and Biomedical Engineering, Nanyang Technological University, 70 Nanyang Drive, 637457, Singapore. E-mail: ChenPeng@ntu.edu.sg; Fax: +65 6791 1761; Tel: +65 6514 1086

[b]School of Physical and Mathematical Sciences, Nanyang Technological University, 21 Nanyang Link, 637371, Singapore

† Electronic supplementary information (ESI) available. See DOI: 10.1039/c5ta01987g

2.2 Materials characterization

The samples were examined with scanning electron microscopy (JSM-6700F, JEOL), Raman spectroscopy (Renishaw InVia Reflex Raman system with a laser excitation wavelength of 514 nm), X-ray diffraction spectroscopy (Bruker D8 Advance Diffractometer using Cu Kα radiation), Fourier transform infrared spectroscopy (PerkinElmer Spectrum GX FTIR system), SEM elemental mapping (JSM-7100F, JEOL), X-ray photoelectron spectroscopy (Kratos Axis Ultra^{DLD} spectrometer with a monochromatized Al Kα X-ray source), Nitrogen adsorption–desorption isotherm (Quantachrome AUTOSORB-1), and transmission electron microscopy (TEM, JEM-3010, with an accelerating voltage of 200 kV, JEOL).

2.3 Electrochemical measurements for ORR

Electrochemical measurements were performed on a CHI-760D electrochemical workstation using a three-electrode configuration with a Pt wire as the counter electrode and an Ag/AgCl electrode as the reference. Cyclic voltammetry (CV) was conducted in KOH (0.1 M) electrolyte in the potential window from −1.0 to 0.2 V at a sweep rate of 10 mV s^{-1}. Using a rotating disk electrode, the polarization curves were obtained at a scan rate of 5 mV s^{-1}, the rotating speed varied from 400 to 2025 rpm, and the potential window was from 0.2 to −0.8 V. Before each measurement, the electrolyte was bubbled with O_2 over 20 min. To prepare the working electrode, 5 mg of carbonized rGO/*E. coli* sample was dispersed into a solution containing 0.9 mL of deionized water and 0.1 mL of 5 wt% Nafion aqueous solution, and ultrasonicated to form a homogenous solution. Subsequently, 20 μL of the obtained solution was deposited onto a glassy carbon electrode (GC, 5 mm in diameter) and dried at 50 °C. A GC electrode coated with commercial Pt/C (20 wt%, Premetek) was measured for comparison. The loading amount of Pt/C was optimized to give the best performance.

2.4 Electrochemical measurements for LIB

The electrochemical performance of carbonized rGO/*E. coli* composite for Li storage was evaluated in 2032 coin-type cells assembled in an argon-filled glove box. To make the LIB anode, carbonaceous rGO/*E. coli* sample, acetylene black, and poly(vinylidene fluoride) with mass ratio of 80 : 10 : 10 were mixed with *N*-methyl-2-pyrrolidone to form a homogeneous slurry, which was then coated onto a copper foil current collector and dried at 100 °C overnight under vacuum. Pure lithium metal served as both a counter electrode and reference electrode. 1 M $LiPF_6$ solution in a mixture of ethylene carbonate and dimethyl carbonate (1 : 1, v/v) served as the electrolyte. The cells were galvanostatically charged and discharged using a Neware battery testing system in the voltage range of 0.005–3.0 V (*vs.* Li/Li$^+$). Cyclic voltammetry (CV) was carried on a CHI-760D electrochemical workstation over a potential window from 0.005 to 3 V at a scan rate of 0.5 mV s^{-1}.

3. Results and discussion

The synthetic procedure for the carbonaceous graphene–bacteria composite is illustrated in Fig. 1. It has been reported that GO sheets with rich oxygenated groups can act as terminal electron acceptors for the bacterial respiration process, leading to their reduction.[17,18] In agreement with this notion, we observe that the yellowish GO dispersion gradually became dark after the addition of *E. coli* bacteria (Fig. S1 in ESI†). The rGO/*E. coli* hybrids collected by centrifugation were subsequently lyophilized and subjected to thermal annealing at 900 °C to carbonize *E. coli* and further reduce rGO sheets.

As revealed by scanning electron microscopy (SEM), the lyophilized rGO/*E. coli* composite is a porous network with numerous *E. coli* cells (∼1 μm) attached onto or encapsulated by the rGO microsheets (Fig. 2a and b). The mild and gradual reduction process allowed for a uniform mixture of *E. coli* and rGO without severe aggregation of the bacteria or rGO sheets. In addition, the bacteria served as spacers to prevent stacking between the hydrophobic rGO sheets. After thermal annealing, the resulting carbonaceous rGO/*E. coli* composite retained the microporous structure except that the carbonized bacteria largely shrunk in size (Fig. 2c and d). As revealed by TEM (Fig. 2e and f), mesopores (<50 nm) appeared on the surface of the carbonized bacteria. Thermal annealing also further reduced rGO, enhanced coupling between rGO and *E. coli*, and possibly induced heteroatom-doping on rGO due to the generation of reactive species from decomposition of the bacterial components.

Raman spectroscopy shows that rGO/*E. coli* exhibits an increased D/G intensity ratio as compared with GO (Fig. 3a). This is attributed to the restoration of graphitic C═C bonds and
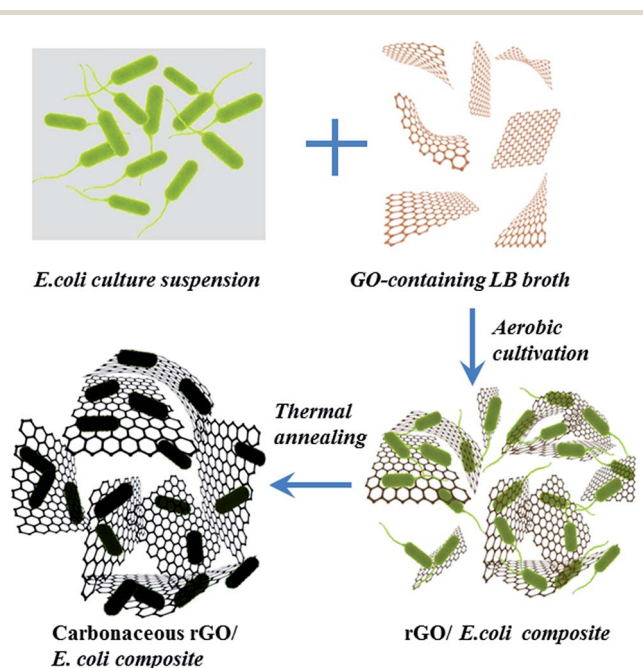

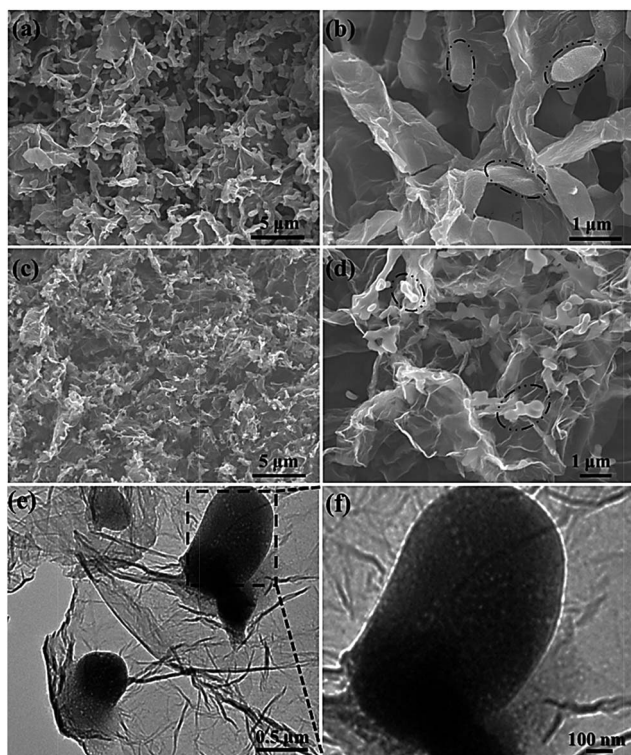**Fig. 1** Schematic of the synthesis of carbonaceous rGO/*E. coli* composite.

Fig. 2 SEM images of rGO/*E. coli* (a and b) before and (c and d) after thermal annealing. The dashed ovals in (b) and (d) highlight the bacterial cells. (e) TEM images of rGO/*E. coli* after thermal annealing. (f) Zoom-in view of a carbonized bacteria in (e).

consequent increase in the number of small sp^2 domains.[19] Both the D and G bands of the carbonaceous rGO/*E. coli* were widened because of the low-crystalline structures from the carbonized bacteria and possibly disorder induced by hetero-atom doping. The X-ray diffraction (XRD) pattern of GO shows a characteristic (002) diffraction peak at 10.74°, indicating an interlayer spacing of ~8.24 Å (Fig. 3b). In addition to the two broad peaks from *E. coli*, the XRD pattern of rGO/*E. coli* also shows a shifted and widened (002) diffraction peak at 24°, corresponding to an interlayer spacing of ~3.71 Å. This confirms the bio-reduction (thus the removal of oxygenated functional groups) of the GO sheets. After thermal annealing, the XRD pattern of carbonaceous rGO/*E. coli* exhibited a broadened characteristic rGO peak at ~25° with much reduced components inherited from *E. coli*. The Fourier transform infrared spectroscopy (FTIR) spectrum of rGO/*E. coli* exhibits characteristic peaks of various functional groups (*e.g.* NH$_2$, C=N, CH$_2$/CH$_3$, P=O, C–O–P, C=O, C–O–C, C=C) from biomolecules in *E. coli* (Fig. 3c).[20] Compared to GO, the C=O peak at 1730 cm^{-1} vanished due to the removal of the COOH groups from the GO sheets after effective bio-reduction.[21] In contrast, the FTIR spectrum of carbonized rGO/*E. coli* presents a dominating graphitic C=C peak at 1626 cm^{-1}, indicating the essential removal of the other chemical groups. Based on a Brunauer–Emmett–Teller (BET) N$_2$ adsorption–desorption measurement (Fig. 3d), the porous structure of carbonized rGO/ *E. coli* specific surface area was 288 m^2 g^{-1}, which is larger than

that of the rGO aerogel obtained by lyophilisation of pure rGO sheets,[22] P-doped graphene[23] and N-, S-codoped graphene obtained by thermal annealing of 2-aminothiophenol func-tionalized GO.[24] Moreover, as shown in Fig. 3d and the (inset), the composite is a mesoporous material with a narrow meso-pore size distribution.

SEM-energy dispersive spectroscopy (SEM-EDS) mapping for the carbonaceous rGO/*E. coli* showed abundant and uniform distribution of C, N, O, and P (Fig. 4a). The observation suggests that these heteroatoms are not only confined in carbonized bacteria but were also uniformly doped onto the rGO sheets. Consistent with this, the X-ray photoelectron spectroscopy (XPS) spectrum possesses the characteristic peaks of P2p at 130 eV, S2p at 164 eV, C1s at 284 eV, N1s at 400 eV and O1s at 532 eV (Fig. 4b).[25,26] The atomic concentrations of N, P and S were 2.42%, 1.25% and 0.42%, respectively. The high resolution N1s spectrum could be deconvoluted into three peaks correspond-ing to pyridinic- (28 at%), pyrrolic- (11 at%) and graphitic- (61 at%) N species (Fig. 4c). The high resolution P2p peak could be resolved into two peaks corresponding to P–C (48.2 at%) and P–O (51.8 at%) (Fig. 4d).[27]

Heteroatom doping endows graphene with catalytic prop-erties. Both N-doped and P-doped graphene have been used for the oxygen reduction reaction (ORR), which is the rate-limiting cathodic reaction in energy devices (*e.g.*, fuel cells, Li–air batteries).[28,29] As shown in Fig. 5a, cyclic voltammetry (CV) of carbonaceous rGO/*E. coli* exhibits a prominent reduction peak in the presence of oxygen, demonstrating its catalytic activity towards the ORR. Fig. 5b depicts linear-sweep vol-tammetry curves at different rotation speeds. The onset potential is ~−0.09 V, which is not far from that of the Pt/C electrode (0 V) and superior to previously reported doped graphene materials.[30–32] Moreover, as shown, the current density reached a steady-state at an overpotential as low as ~0.38 V even at the high rotation speed of 1600 rpm, implying a high efficiency of the ORR. The slight decrease of current density at high overpotentials (>0.6 V) is because the replen-ishment of oxygen by diffusion lags behind the rapid reduc-tion reaction.[33]

The electron transfer kinetics were analysed using a Kou-tecky–Levich (K–L) plot at the potential of −0.4 V (Fig. 5c). The good linear fit signifies a first order reaction and its slope indicates an electron-transfer number of 3.95 (derivation in ESI†). Such an efficient four-electron process was preserved even at a high overpotential (0.8 V). As shown in Fig. S3 (ESI†), rGO/*E. coli* and Pt/C exhibit comparable Tafel slopes at low current values, indicating that the rate-limiting step for both materials at low currents is the first electron transfer step and confirming similar electrocatalytic activity for both materials.[34] The excellent electrocatalytic property of the carbonaceous rGO/ *E. coli* composite is attributed to the enriched and well-exposed active sites and the synergistic effects of multiple dopants. The co-existence of multiple species of heteroatoms can introduce asymmetric spins and charge polarization in a graphene lattice thereby improving the electrocatalytic activity.[13,35,36] For example, it has been reported that introducing S and O atoms into N-doped nanoporous carbon further enhances its
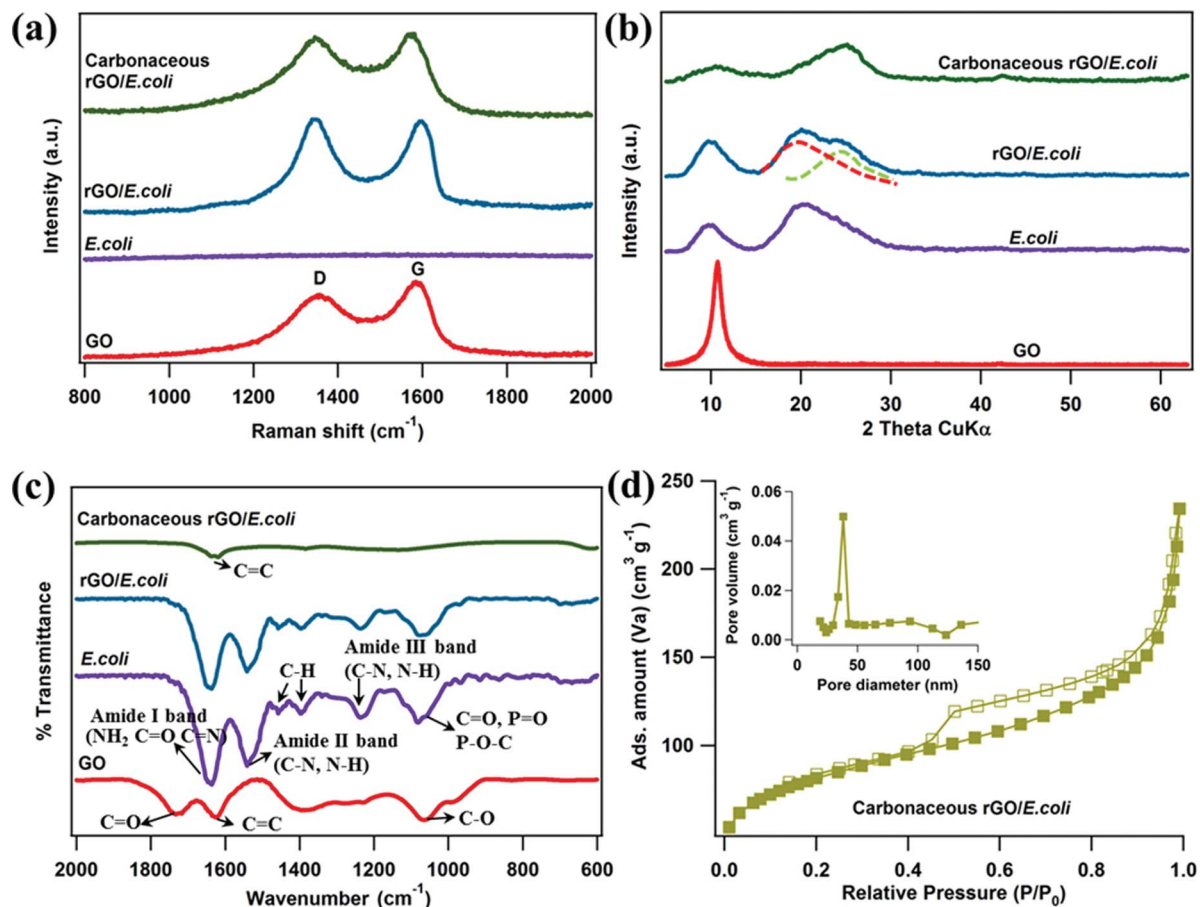
Fig. 3 (a) Raman spectra, (b) XRD patterns, (c) FTIR spectra, (d) nitrogen adsorption and desorption isotherm of the prepared samples. Inset in (d) shows the pore size distribution of the carbonaceous rGO/*E. coli* composite.

electrocatalytic activity towards ORR.[37] The performance of rGO/*E. coli* was superior to the previously reported ternary (N,P,B)-doped porous nanocarbons,[38] N and S co-doped graphene,[24] N-doped graphene,[30] and sulfonic acid-functionalized graphene nanoplates.[39]

Although the onset potential of carbonaceous rGO/*E. coli* is not as ideal as Pt/C (Fig. S2 in ESI†), it exhibits better durability because of its higher resistance to electrochemical oxidation (Fig. 5d). Methanol is a readily available and a widely used fuel for fuel cells. However, the commercialization of direct
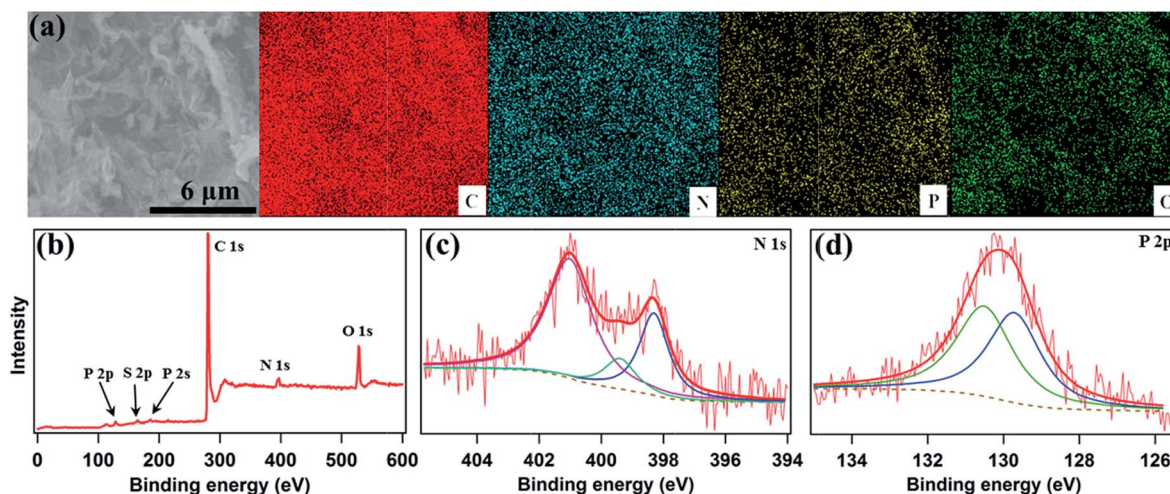

Fig. 4 (a) SEM-EDS mapping, and (b–d) XPS analyses of the carbonaceous rGO/*E. coli* composite.
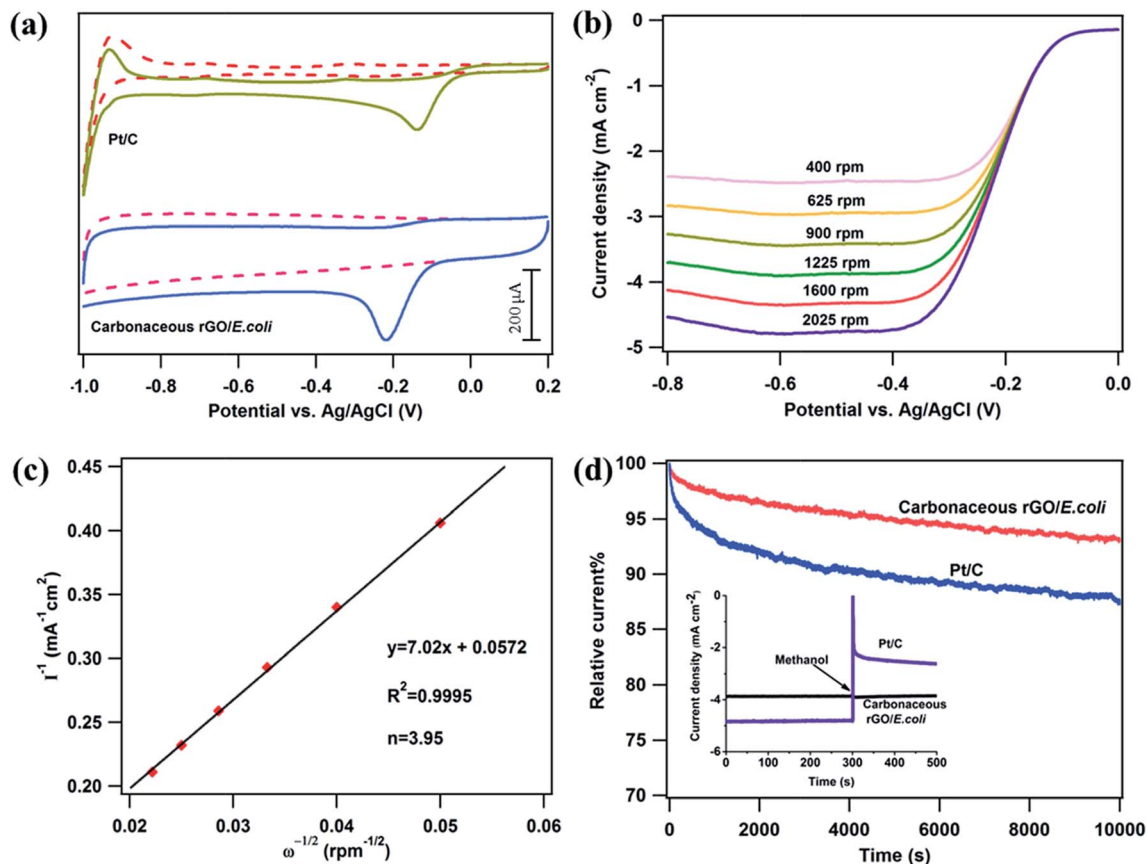
Fig. 5 (a) CV curves of carbonaceous rGO/*E. coli* and Pt/C in O_2-saturated (solid line) and N_2-saturated (dashed line) 0.1 M KOH solutions with a scan rate of 10 mV s^{-1}. (b) RDE (rotating disk electrode) voltammograms of carbonaceous rGO/*E. coli* in O_2-saturated 0.1 M KOH at a scan rate of 5 mV s^{-1} and various rotation speeds. (c) Koutecky–Levich (K–L) plot at −0.4 V *vs.* Ag/AgCl. (d) Normalized chronoamperometric curves of carbonaceous rGO/*E. coli* and commercial Pt/C at −0.4 V *vs.* Ag/AgCl in O_2-saturated 0.1 M KOH solution. Inset shows the interference by addition of 2% v/v methanol.

methanol fuel cells is seriously hindered by the toxification of platinum by methanol crossover from anode to cathode through the membrane. In contrast, our rGO/*E. coli* shows remarkable tolerance to methanol (Fig. 5d, inset).

Heteroatom-doped graphene nanomaterials have also been considered as promising electrode materials for lithium ion batteries (LIB).[40] Fig. 6a depicts the first five CVs of carbonized rGO/*E. coli* as the anode material for LIB. The strong reduction peak at 0.5–1.0 V in the first cycle is an indicator of the formation of a solid-electrolyte interphase (SEI) film on the electrode surface.[27] Notably, there are a few small redox peaks (specifically, oxidation peaks at *ca.* 1.2, 1.8 and 2.4 V, reduction peaks at *ca.* 1.3, 1.7 and 2.1 V) in the first two cycles, which likely resulted from the irreversible binding and delithiation of Li ions caused by defects, dopants and oxygen-containing functional groups on the carbonaceous rGO/*E. coli* composite.[13] From the third cycle onwards, the CV curves overlap demonstrating the good stability and reversibility of the electrode.

As shown in Fig. 6b, carbonaceous rGO/*E. coli* shows an initial discharge capacity of 1048 mA h g^{-1} and a reversible capacity of 587 mA h g^{-1} at current density of 0.5 C (1 C means the theoretical capacity of graphite, 372 mA h g^{-1}, can be

charged or discharged within 1 h). The plateau in the discharge profile at ∼0.9 V can be ascribed to the formation of an SEI film on the electrode surface. The irreversible capacity loss in the first cycle is ascribed to the consumption of Li by defects and dopants, the initial formation of SEI, as well as the electrolyte decomposition. After the initial decrease, the discharging capacity of rGO/*E. coli* electrode gradually increased reaching a value of 501.5 mA h g^{-1} at the 380th cycle (Fig. 6c). The increase of the discharging capacity may be attributed to the electrochemical activation of electrode materials and/or enhanced accessibility of Li ions during cycling. This observation indicates the remarkable cycling stability of the electrode. The Coulombic efficiency was retained at 97–99% from the 5th cycle onwards. Fig. 6d presents the rate performance of the rGO/*E. coli* electrode at 0.2 to 0.5, 1, 2, 5 and 10 C. This heteroatom-doped electrode outperformed the previously reported undoped 3D graphene (308 mA h g^{-1} at 50 mA g^{-1}),[41] N-doped graphene (∼200 mA h g^{-1} at 2 C),[42] P-doped graphene (∼200 mA h g^{-1} at 2 A g^{-1}),[27] and phenolic resin-grafted rGO (212.3 mA h g^{-1} at 2 A g^{-1}).[43] In addition, the capacity can be completely restored once the current rate returns to the initial 0.2 C. Taken together, our electrode demonstrated excellent rate performance and reversibility.
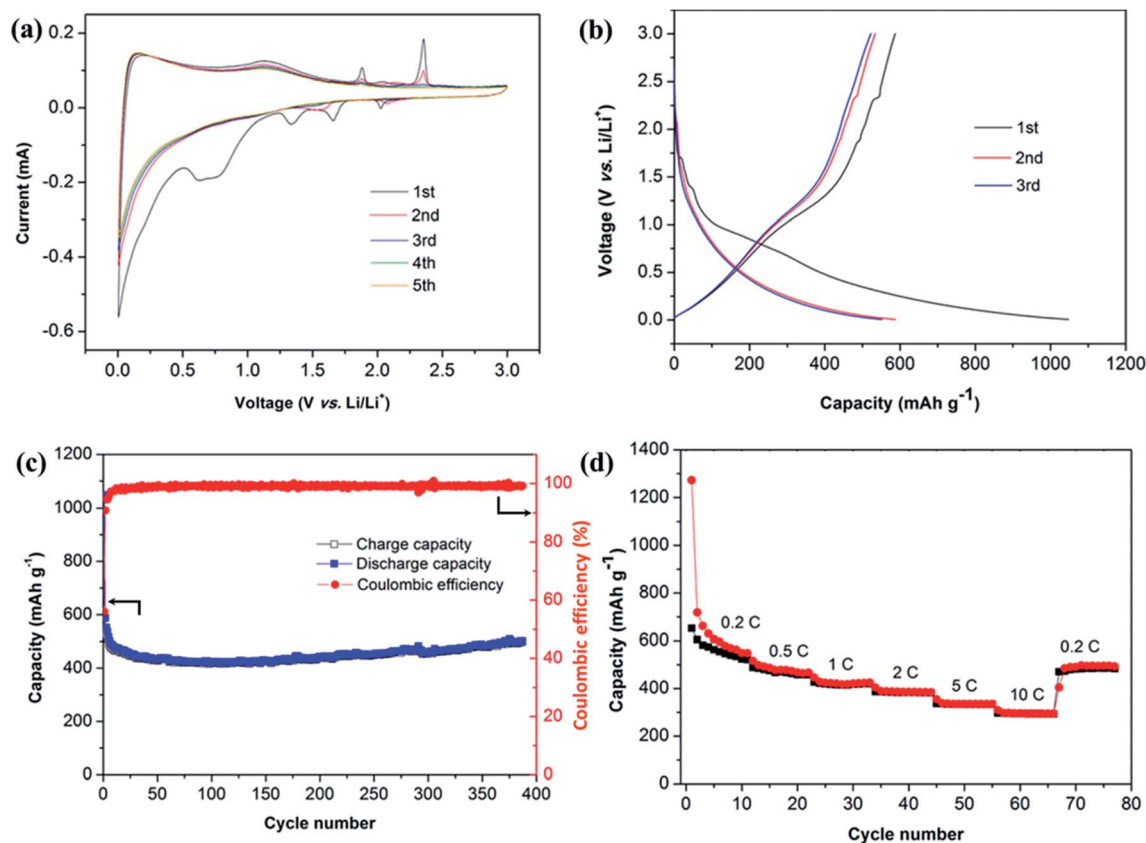
Fig. 6 (a) CV curves of carbonaceous rGO/*E. coli* at a scan rate of 0.5 mV s^{-1}. (b) Galvanostatic charge−discharge profiles at current density of 0.5 C. (c) Cycling performance and Coulombic efficiency of rGO/*E. coli* electrode at 0.5 C between 0.005 and 3 V *vs.* Li$^+$/Li. (d) Rate performance of rGO/*E. coli* electrode charged between 0.005 and 3 V *vs.* Li$^+$/Li at various current densities.

4. Conclusions

In summary, a hybrid graphene structure doped with multiple heteroatom species has been fabricated by a facile and green method using bacteria as the reducing agent, spacer, and doping source. Such an rGO/*E. coli* composite promises a wide range of applications, including electrocatalysis, sensing, energy storage and conversion. For proof-of-concept demonstrations, we showed its superior performance in the oxygen reduction reaction and lithium ion batteries. This is attributed to the excellent catalytic and electrochemical activities endowed by the synergistic effects of co-dopants. In addition, the porous structure of the composite offers a large surface area, good ion accessibility, and abundant active edge sites.

Acknowledgements

Notes and references

1 J. Liu, *Nat. Nanotechnol.*, 2014, **9**, 739–741.

2 F. Bonaccorso, L. Colombo, G. H. Yu, M. Stoller, V. Tozzini, A. C. Ferrari, R. S. Ruoff and V. Pellegrini, *Science*, 2015, **347**, 6217.

3 S. Han, D. Q. Wu, S. Li, F. Zhang and X. L. Feng, *Adv. Mater.*, 2014, **26**, 849–864.

4 S. J. Guo and S. H. Sun, *J. Am. Chem. Soc.*, 2012, **134**, 2492–2495.

5 X. J. Zhou, J. L. Qiao, L. Yang and J. J. Zhang, *Adv. Energy Mater.*, 2014, **4**, 130523.

6 X. S. Zhou, L. J. Wan and Y. G. Guo, *Adv. Mater.*, 2013, **25**, 2152–2157.

7 W. W. Sun and Y. Wang, *Nanoscale*, 2014, **6**, 11528–11552.

8 S. Bag, K. Roy, C. S. Gopinath and C. R. Raj, *ACS Appl. Mater. Interfaces*, 2014, **6**, 2692–2699.

9 J. W. Lee, S. Y. Lim, H. M. Jeong, T. H. Hwang, J. K. Kang and J. W. Choi, *Energy Environ. Sci.*, 2012, **5**, 9889–9894.

10 S. Mayavan, H. S. Jang, M. J. Lee, S. H. Choi and S. M. Choi, *J. Mater. Chem. A*, 2013, **1**, 3489–3494.

11 D. P. Dubal, R. Holze and P. Gomez-Romero, *Sci. Rep.*, 2014, **4**, 7349.

12 S. Chen and S. Z. Qiao, *ACS Nano*, 2013, 7, 10190–10196.

13 X. W. Wang, G. Z. Sun, P. Routh, D. H. Kim, W. Huang and P. Chen, *Chem. Soc. Rev.*, 2014, **43**, 7067–7098.

14 X. K. Kong, C. L. Chen and Q. W. Chen, *Chem. Soc. Rev.*, 2014, **43**, 2841–2857.

15 A. Dhakshinamoorthy, A. Primo, P. Concepcion, M. Alvaro and H. Garcia, *Chem.–Eur. J.*, 2013, **19**, 7547–7554.

16 S. L. Ting, C. X. Guo, K. C. Leong, D. H. Kim, C. M. Li and P. Chen, *Electrochim. Acta*, 2013, **111**, 441–446.

17 S. Gurunathan, J. W. Han, V. Eppakayala and J. H. Kim, *Colloids Surf., B*, 2013, **102**, 772–777.

18 G. M. Wang, F. Qian, C. Saltikov, Y. Q. Jiao and Y. Li, *Nano Res.*, 2011, **4**, 563–570.

19 H. B. Feng, R. Cheng, X. Zhao, X. F. Duan and J. H. Li, *Nat. Commun.*, 2013, **4**, 1539.

20 Z. Filip, S. Hermann and K. Demnerova, *Czech J. Food Sci.*, 2008, **26**, 458–463.

21 Z. Z. Du, W. Li, W. Ai, Q. Tai, L. H. Xie, Y. Cao, J. Q. Liu, M. D. Yi, H. F. Ling, Z. H. Li and W. Huang, *RSC Adv.*, 2013, **3**, 25788–25791.

22 W. F. Chen, S. R. Li, C. H. Chen and L. F. Yan, *Adv. Mater.*, 2011, **23**, 5679–5683.

23 Y. Y. Wen, B. Wang, C. C. Huang, L. Z. Wang and D. Hulicova-Jurcakova, *Chem.–Eur. J.*, 2015, **21**, 80–85.

24 W. Ai, Z. M. Luo, J. Jiang, J. H. Zhu, Z. Z. Du, Z. X. Fan, L. H. Xie, H. Zhang, W. Huang and T. Yu, *Adv. Mater.*, 2014, **26**, 6186–6192.

25 A. G. Kannan, J. Zhao, S. G. Jo, Y. S. Kang and D. W. Kim, *J. Mater. Chem. A*, 2014, **2**, 12232–12239.

26 J. S. Li, S. L. Li, Y. J. Tang, K. Li, L. Zhou, N. Kong, Y. Q. Lan, J. C. Bao and Z. H. Dai, *Sci. Rep.*, 2014, **4**, 5130.

27 C. Z. Zhang, N. Mahmood, H. Yin, F. Liu and Y. L. Hou, *Adv. Mater.*, 2013, **25**, 4932–4937.

28 R. Li, Z. D. Wei, X. L. Gou and W. Xu, *RSC Adv.*, 2013, **3**, 9978–9984.

29 M. Borghei, I. Azcune, P. M. Carrasco, J. Sainio, E. Kauppinen and V. Ruiz, *Int. J. Hydrogen Energy*, 2014, **39**, 12749–12756.

30 Y. W. Zhang, J. Ge, L. Wang, D. H. Wang, F. Ding, X. M. Tao and W. Chen, *Sci. Rep.*, 2013, **3**, 2771.

31 F. X. Ma, J. Wang, F. B. Wang and X. H. Xia, *Chem. Commun.*, 2015, **51**, 1198–1201.

32 Y. Z. Su, Y. Zhang, X. D. Zhuang, S. Li, D. Q. Wu, F. Zhang and X. L. Feng, *Carbon*, 2013, **62**, 296–301.

33 J. Liang, Y. Zheng, J. Chen, J. Liu, D. Hulicova-Jurcakova, M. Jaroniec and S. Z. Qiao, *Angew. Chem., Int. Ed.*, 2012, **51**, 3892–3896.

34 C. J. Song and J. J. Zhang, *PEM Fuel Cell Electrocatalysts and Catalyst Layers*, ed. J. J. Zhang, Springer, London, 2008, pp. 89–134.

35 I. Y. Jeon, H. J. Choi, M. Choi, J. M. Seo, S. M. Jung, M. J. Kim, S. Zhang, L. P. Zhang, Z. H. Xia, L. M. Dai, N. Park and J. B. Baek, *Sci. Rep.*, 2013, **3**, 1810.

36 I. Y. Jeon, S. Zhang, L. P. Zhang, H. J. Choi, J. M. Seo, Z. H. Xia, L. M. Dai and J. B. Baek, *Adv. Mater.*, 2013, **25**, 6138–6145.

37 Y. Y. Meng, D. Voiry, A. Goswami, X. X. Zou, X. X. Huang, M. Chhowalla, Z. W. Liu and T. Asefa, *J. Am. Chem. Soc.*, 2014, **136**, 13554–13557.

38 S. Y. Zhao, J. Liu, C. X. Li, W. B. Ji, M. M. Yang, H. Huang, Y. Liu and Z. H. Kang, *ACS Appl. Mater. Interfaces*, 2014, **6**, 22297–22304.

39 I. Y. Jeon, H. J. Choi, S. M. Jung, J. M. Seo, M. J. Kim, L. M. Dai and J. B. Baek, *J. Am. Chem. Soc.*, 2013, **135**, 1386–1393.

40 B. Quan, S. H. Yu, D. Y. Chung, A. H. Jin, J. H. Park, Y. E. Sung and Y. Z. Piao, *Sci. Rep.*, 2014, **4**, 5639.

41 C. X. Guo, M. Wang, T. Chen, X. W. Lou and C. M. Li, *Adv. Energy Mater.*, 2011, **1**, 736–741.

42 M. Du, J. Sun, J. Chang, F. Yang, L. J. Shi and L. Gao, *RSC Adv.*, 2014, **4**, 42412–42417.

43 M. C. Li, H. H. Song, X. H. Chen, J. S. Zhou and Z. K. Ma, *Phys. Chem. Chem. Phys.*, 2015, **17**, 3250–3260.